Spin-Orbit-Induced Strong Coupling of a Single Spin to a Nanomechanical Resonator

András Pályi,[1,2] P. R. Struck,[1] Mark Rudner,[3] Karsten Flensberg,[3,4] and Guido Burkard[1]

[1]*Department of Physics, University of Konstanz, D-78457 Konstanz, Germany*
[2]*Department of Materials Physics, Eötvös University, H-1517 Budapest POB 32, Hungary*
[3]*Department of Physics, Harvard University, Cambridge, Massachusetts 02138, USA*
[4]*Niels Bohr Institute, University of Copenhagen, Universitetsparken 5, DK-2100 Copenhagen, Denmark*

(Received 24 October 2011; published 18 May 2012)

We theoretically investigate the deflection-induced coupling of an electron spin to vibrational motion due to spin-orbit coupling in suspended carbon nanotube quantum dots. Our estimates indicate that, with current capabilities, a quantum dot with an odd number of electrons can serve as a realization of the Jaynes-Cummings model of quantum electrodynamics in the strong-coupling regime. A quantized flexural mode of the suspended tube plays the role of the optical mode and we identify two distinct two-level subspaces, at small and large magnetic field, which can be used as qubits in this setup. The strong intrinsic spin-mechanical coupling allows for detection, as well as manipulation of the spin qubit, and may yield enhanced performance of nanotubes in sensing applications.

DOI: 10.1103/PhysRevLett.108.206811 PACS numbers: 73.63.Fg, 62.25.−g, 71.70.Ej, 73.63.Kv

Recent experiments in nanomechanics have reached the ultimate quantum limit by cooling a nanomechanical system close to its ground state [1]. Among the variety of available nanomechanical systems, nanostructures made out of atomically-thin carbon-based materials such as graphene and carbon nanotubes (CNTs) stand out due to their low masses and high stiffnesses. These properties give rise to high oscillation frequencies, potentially enabling near ground-state cooling using conventional cryogenics, and large zero-point motion, which improves the ease of detection [2,3].

Recently, a high quality-factor suspended CNT resonator was used to demonstrate strong coupling between nanomechanical motion and single-charge tunneling through a quantum dot (QD) defined in the CNT [4]. Here, we theoretically investigate the coupling of a single electron spin to the quantized motion of a discrete flexural mode of a suspended CNT (see Fig. 1), and show that the strong-coupling regime of this Jaynes-Cummings-type system is within reach. This coupling provides means for electrical manipulation of the electron spin via microwave irradiation, and leads to strong nonlinearities in the CNT's mechanical response which may potentially be used for enhanced functionality in sensing applications [5–7].

In addition to their outstanding mechanical properties, carbon-based systems also possess many attractive characteristics for information processing applications. The potential for single electron spins in QDs to serve as the elementary qubits for quantum information processing [8] is currently being investigated in a variety of systems. In many materials, such as GaAs, the hyperfine interaction between electron and nuclear spins is the primary source of electron spin decoherence which limits qubit performance (see, e.g., [9]). However, carbon-based structures can be grown using starting materials isotopically-enriched in ^{12}C, which has no net nuclear spin, thus practically eliminating the hyperfine mechanism of decoherence [10], leaving behind only a spin-orbit contribution [11,12]. Furthermore, while the phonon continuum in bulk materials provides the primary bath enabling spin relaxation, the discretized phonon spectrum of a suspended CNT can be engineered to have an extremely low density of states at the qubit (spin) energy splitting. Thus very long spin lifetimes are expected off-resonance [13]. On the other hand, when the spin splitting is nearly resonant with one of the high-Q discrete phonon "cavity" modes, strong spin-phonon coupling can enable qubit control, information transfer, or the preparation of entangled states.

The interaction between nanomechanical resonators and single spins was recently detected [14], and has been theoretically investigated [15,16] for cases where the spin-resonator coupling arises from the relative motion of the spin and a source of local magnetic field gradients.

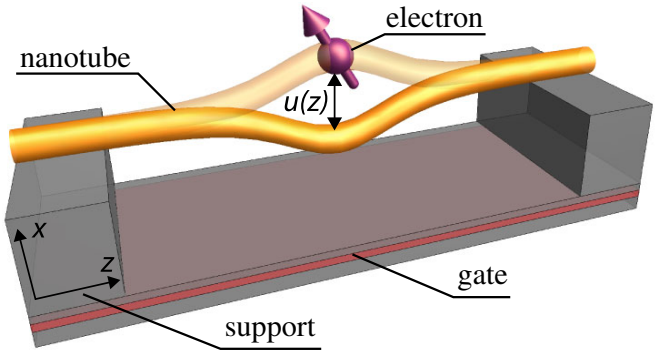

FIG. 1 (color online). Schematic of a suspended CNT containing a quantum dot filled with a single electron spin. The spin-orbit coupling in the CNT induces a strong coupling between the spin and the quantized mechanical motion of the CNT.

Such coupling is achieved, e.g., using a magnetic tip on a vibrating cantilever which can be positioned close to an isolated spin fixed to a nonmoving substrate. Creating strong, well-controlled, local gradients remains challenging for such setups. In contrast, as we now describe, in CNTs the spin-mechanical coupling is *intrinsic*, supplied by the inherent strong spin-orbit coupling [17–20] which was recently discovered by Kuemmeth *et al.* [21].

Consider an electron localized in a suspended CNT quantum dot (see Fig. 1). Below we focus on the case of a single electron, but expect the qualitative features to be valid for any odd occupancy (see Ref. [22]). We work in the experimentally relevant parameter regime where the spin-orbit and orbital-Zeeman couplings are small compared with the nanotube band gap and the energy of the longitudinal motion in the QD. Here, the longitudinal and sublattice orbital degrees of freedom are effectively frozen out, leaving behind a nominally fourfold degenerate low-energy subspace associated with the remaining spin and valley degrees of freedom (see Refs. [23,24]).

A simple model describing the spin and valley dynamics in this low-energy QD subspace, incorporating the coupling of electron spin to deflections associated with the flexural modes of the CNT [25,26], was introduced in Ref. [27]. In principle, the deformation-potential spin-phonon coupling mechanism [11] is also present. The deflection coupling mechanism is expected to dominate at long phonon wavelengths, while the deformation-potential coupling should dominate at short wavelengths (see discussion in [27]). For simplicity we consider only the deflection coupling mechanism, but note that the approach can readily be extended to include both effects.

The Hamiltonian describing this system is [24,27,28]

$$H = \frac{\Delta_{\rm so}}{2}\tau_3(\mathbf{s}\cdot\mathbf{t}) + \Delta_{KK'}\tau_1 - \mu_{\rm orb}\tau_3(\mathbf{B}\cdot\mathbf{t}) + \mu_B(\mathbf{s}\cdot\mathbf{B}), \tag{1}$$

where $\Delta_{\rm so}$ and $\Delta_{KK'}$ denote the spin-orbit and intervalley couplings, τ_i and s_i are the Pauli matrices in valley and spin space (the pseudospin is frozen out for the states localized in a QD), $\mathbf{t}$ is the tangent vector along the CNT axis, and $\mathbf{B}$ denotes the magnetic field. Note that the spin-orbit coupling has contributions which are diagonal and off-diagonal in sublattice space [18–20,22]. When projected onto to a single longitudinal mode of the quantum dot, the effective Hamiltonian given above describes the coupling of the spin to the nanotube deflection at the location of the dot [24].

For a nominally straight CNT we take $\mathbf{t}$ pointing along the z direction, giving $\mathbf{s}\cdot\mathbf{t} = s_z$ and $\mathbf{B}\cdot\mathbf{t} = B_z$. Here we find the low-energy spectrum shown in Fig. 2. The two boxed regions indicate two different two-level systems that can be envisioned as qubit implementations in this setup: we define a spin qubit [8] (S) at strong longitudinal magnetic field, near the value B^* of the upper level crossing,

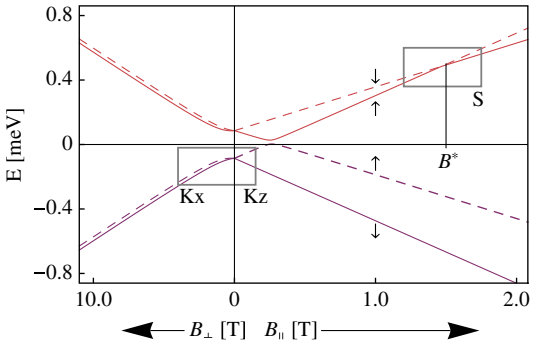

FIG. 2 (color online). Energy levels of the four dimensional (due to spin and valley) orbital ground state subspace of the QD, as a function of the magnetic field parallel ($B_\parallel$) and perpendicular ($B_\perp$) to the CNT axis. The boxed areas indicate the working regime for the spin qubit (S) and Kramers qubit (K), the latter being operated either in a longitudinal (Kz) or perpendicular (Kx) magnetic field. Parameter values [30]: $\Delta_{\rm so} = 170\ \mu$eV, $\Delta_{KK'} = 12.5\ \mu$eV, $\mu_{\rm orb} = 330\ \mu$eV/T.

and a mixed spin-valley or Kramers (K) qubit [28], which can be operated at low fields applied either in the longitudinal (Kz) or perpendicular (Kx) directions.

We now study how these qubits couple to the quantized mechanical motion of the CNT. For simplicity we consider only a single polarization of flexural motion (along the x direction), assuming that the two-fold degeneracy is broken, e.g., by an external electric field. A generalization to two modes is straightforward.

A generic deformation of the CNT with deflection $u(z)$ makes the tangent vector $\mathbf{t}(z)$ coordinate-dependent. Expanding $\mathbf{t}(z)$ for small deflections, we rewrite the coupling terms in Hamiltonian (1) as $\mathbf{s}\cdot\mathbf{t} \simeq s_z + (du/dz)s_x$ and $\mathbf{B}\cdot\mathbf{t} \simeq B_z + (du/dz)B_x$. Expressing the deflection $u(z)$ in terms of the creation and annihilation operators $a^\dagger$ and a for a quantized flexural phonon mode, $u(z) = f(z)\frac{\ell_0}{\sqrt{2}}(a + a^\dagger)$, where $f(z)$ and ℓ_0 are the waveform and zero-point amplitude of the phonon mode, we find that each of the three qubit types (S, Kx, Kz) obtains a coupling to the oscillator mode which we describe as

$$\frac{H}{\hbar} = \frac{\omega_q}{2}\sigma_3 + g(a + a^\dagger)\sigma_1 + \omega_p a^\dagger a + 2\lambda(a + a^\dagger)\cos\omega t. \tag{2}$$

Here the matrices $\sigma_{1,3}$ are Pauli matrices acting on the two-level qubit subspace, and we have included a term describing external driving of the oscillator with frequency ω and coupling strength λ, which can be achieved by coupling to the ac electric field of a nearby antenna [4]. Below we describe the dependence of the qubit-oscillator coupling g on system parameters for each qubit type (S, Kx, or Kz). The derivation of Eq. (2) is detailed in [24].

For the spin qubit (S), the relevant twofold degree of freedom is the spin of the electron itself. Therefore in

Eq. (2) we have $\sigma_3 = s_z$ and $\sigma_1 = s_x$, and the qubit levels are split by the Zeeman energy, measured relative to the value B^* where the spin-orbit-split levels cross, $\hbar\omega_q = \mu_B(B - B^*)$. A spin magnetic moment of μ_B is assumed, and $B^* \approx \Delta_{\rm so}/2\mu_B$ for $\Delta_{KK'} \ll \Delta_{\rm so}$. For the qubit-resonator coupling, we find $g = \Delta_{\rm so}\langle f'\rangle\ell_0/2\sqrt{2}$, independent of B. Here, $\langle f'\rangle$ is the derivative of the waveform of the phonon mode averaged against the electron density profile in the QD.

For a symmetric QD, positioned at the midpoint of the CNT, the coupling matrix element proportional to $\langle f'\rangle$ vanishes for the fundamental and all even harmonics (the opposite would be true for the deformation-potential coupling mechanism). The cancellation is avoided for a QD positioned away from the symmetry point of the CNT, or for coupling to odd harmonics. Here, for concreteness, we consider coupling of a symmetric QD to the first vibrational harmonic of the CNT. Using realistic parameter values [4,21,29,30], $L = 400$ nm, $\ell_0 = 2.5$ pm, $\Delta_{\rm so} = 370$ μeV, $\Delta_{KK'} = 32.5$ μeV, $\mu_{\rm orb} = 1550$ μeV/T, and $\omega_p/2\pi = 500$ MHz, we find $g/2\pi \approx 0.56$ MHz, irrespective of the magnetic field strength B along the CNT.

For the Kramers qubits (Kx and Kz), both ω_q and g depend on B. The qubit splitting for the Kx qubit is controlled by the perpendicular field, $\hbar\omega_q = \mu_B(2\Delta_{KK'}/\Delta)B_x$, while for the Kz qubit, it is controlled by the longitudinal field $\hbar\omega_q = (\mu_B + \mu_{\rm orb}(\Delta_{\rm so}/\Delta))B_z$, where $\Delta = \sqrt{\Delta_{\rm so}^2 + 4\Delta_{KK'}^2}$ denotes the zero-field splitting between the two Kramers pairs. Resonant coupling occurs when $\omega_q = \omega_p$. This condition sets the relevant value of B_x (B_z) in the case of the Kx (Kz) qubit; the parameters above yield $B_x \approx 103$ mT ($B_z \approx 0.6$ mT).

The qubit-cavity coupling for the Kx qubit increases linearly with the applied perpendicular field, $\hbar g = -(\langle f'\rangle\ell_0/\sqrt{2})(\mu_{\rm orb}\Delta_{\rm so}/\Delta + \mu_B\Delta_{\rm so}^2/\Delta^2)B_x$, while for the Kz qubit it scales with the longitudinal field, $\hbar g = (\langle f'\rangle\ell_0/\sqrt{2})(\mu_{\rm orb}2\Delta_{KK'}\Delta_{\rm so}/\Delta^2)B_z$. Using the values of B_x and B_z obtained above, we estimate couplings of $g/2\pi \approx 0.49$ MHz for the Kx qubit, and $g/2\pi \approx 0.52$ kHz for the Kz qubit. Thus the coupling for the Kx qubit is comparable to that of the spin qubit, while the coupling of the Kz qubit is much weaker. Therefore, we restrict our considerations to the spin and Kx qubits below.

Ref. [4] reports the fabrication of CNT resonators with quality factors $Q \approx 150,000$. We take $Q = 63,000$ for the following estimate. Together with the oscillator frequency $\omega_p/2\pi = 500$ MHz, this value of Q implies an oscillator damping rate of $\Gamma \approx 5 \times 10^4$ s$^{-1} \ll g$. Because of the near-zero density of states of other phonon modes at ω_q, it is reasonable to assume a very low spontaneous qubit relaxation rate γ. These observations suggest that the so-called ''strong coupling'' regime of qubit-oscillator interaction, defined as $\Gamma, \gamma \ll g$, can be reached with CNT resonators.

To quantify the system's response in the anticipated parameter regime, we study the coupled qubit-oscillator dynamics using a master equation which takes into account the finite lifetime of the phonon mode as well as the nonzero temperature of the external phonon bath. For weak driving, $\lambda \ll \omega_p$, and $\omega_p \approx \omega_q \approx \omega \gg g$, we move to a rotating frame and use the rotating wave approximation (RWA) to map the Hamiltonian, Eq. (2), into Jaynes-Cummings form [31]

$$\frac{H_{\rm RWA}}{\hbar} = \frac{\tilde{\omega}_q}{2}\sigma_3 + g(a\sigma_+ + a^\dagger\sigma_-) + \tilde{\omega}_p a^\dagger a + \lambda(a + a^\dagger), \tag{3}$$

where $\tilde{\omega}_i = \omega_i - \omega$. Including the nonunitary dynamics associated with the phonon-bath coupling, the master equation for the qubit-oscillator density matrix ρ reads:

$$\dot{\rho} = -\frac{i}{\hbar}[H_{\rm RWA}, \rho] + (n_B + 1)\Gamma\left(a\rho a^\dagger - \frac{1}{2}\{a^\dagger a, \rho\}\right) + n_B\Gamma\left(a^\dagger\rho a - \frac{1}{2}\{aa^\dagger, \rho\}\right), \tag{4}$$

where $n_B = 1/(e^{\hbar\omega_p/k_BT} - 1)$ is the bath-mode Bose-Einstein occupation factor, and k_B is the Boltzmann constant.

Because of the phonon damping, in the long-time limit the system is expected to tend towards a steady state, described by the density matrix $\bar{\rho}$. We study these steady states, found by setting $\dot{\rho} = 0$ in Eq. (4), using both numerical and semiclassical analytical methods. In Figs. 3(a) and 3(c) we show the steady-state phonon occupation probability distribution $P(\delta\omega, n)$ as a function of the drive frequency-phonon frequency detuning $\delta\omega = -\tilde{\omega}_p$ and the phonon occupation number n, for the case where the qubit and oscillator frequencies are fixed and degenerate, $\omega_q = \omega_p$ (see caption for parameter values). Panels a and c compare the cases with and without qubit-oscillator coupling. In Figs. 3(b) and 3(d) we show the averaged phonon occupation number $\bar{n}(\delta\omega) = \sum_n nP(\delta\omega, n)$, which is closely related to the mean squared resonator displacement in the steady state: $X^2 = x^2 = \ell_0^2(\bar{n} + \frac{1}{2})$. For $g \neq 0$, we observe a splitting of the oscillator resonance, which is characteristic of the coupling to the two-level system, and can serve as an experimental signature of the qubit-oscillator coupling. For drive frequencies near the split peaks, the phonon number distribution is bimodal [Fig. 3(f)] showing peaks at $n \approx 0$ and at high-n, indicating bistable behavior (see below).

For strong excitation, where the mean phonon occupation is large, we expect a semiclassical approach to capture the main features of the system's dynamics [32,33]. Extending the approach described in [32] to include distinct values of the qubit, oscillator, and drive frequencies, ω_q, ω_p, and ω, we derive semiclassical equations of mo-

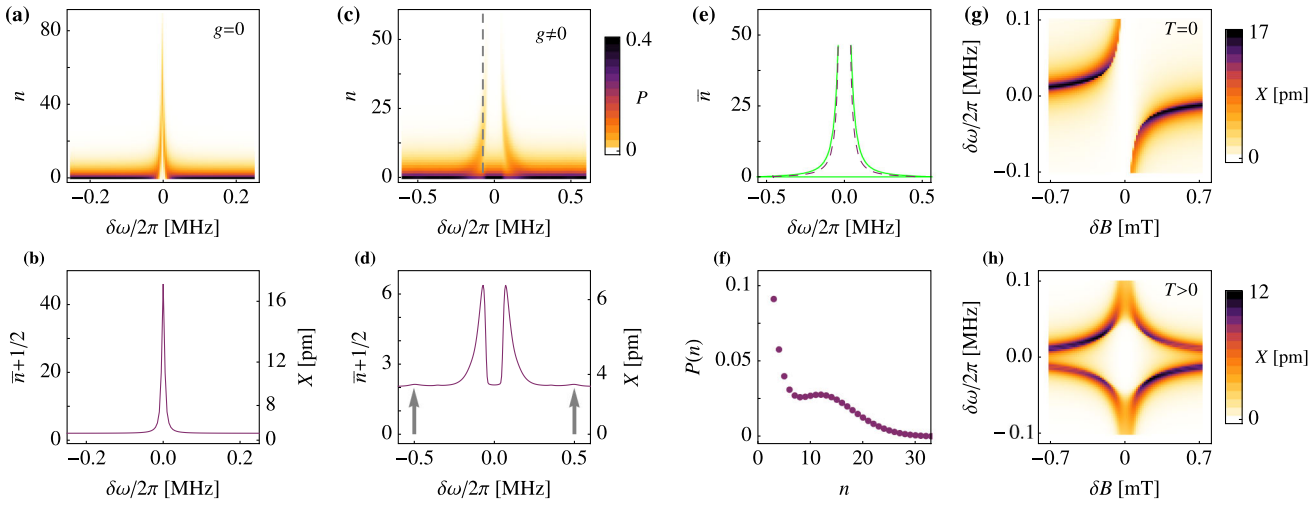

FIG. 3 (color online). Response of the spin-oscillator system. (a) Phonon number probability distribution $P(n, \delta\omega)$, (b) average phonon occupation $\bar{n}$ and root mean squared displacement X of the uncoupled driven CNT resonator ($g = 0$), as functions of the drive frequency—oscillator frequency detuning $\delta\omega = \omega - \omega_p$. The parameters are $T = 50$ mK, $\omega_p/2\pi = 500$ MHz, $\Gamma = 5 \times 10^4$ s^{-1} and $\lambda/2\pi = 0.027$ MHz. The same quantities are plotted in (c) and (d) for a resonantly coupled qubit-oscillator system (i.e., $\omega_q = \omega_p$), with coupling constant $g/2\pi = 0.5$ MHz and further parameters as in (a) and (b). (e) Steady-state oscillator response from the semiclassical calculation, corresponding to the parameters of (c) and (d). The green solid (purple dashed) lines describe stable (unstable) solutions. (f) Bimodal phonon number distribution, taken along the dashed vertical line of (c). (g,h) Root mean squared value X of the resonator amplitude in the coupled spin qubit-oscillator system at (g) $T = 0$ and (h) $T = 50$ mK, as functions of magnetic field detuning δB (detuning the qubit frequency away from resonance with the oscillator) and drive frequency-oscillator frequency detuning $\delta\omega$.

tion for the mean spin and oscillator variables (see [24]). The steady-state values of the mean squared oscillator amplitude obtained from the resulting nonlinear system are shown in Fig. 3(e). In the vicinity of the split peak we find two branches of stable steady-state solutions, indicative of bistable or hysteretic behavior [4]. The semiclassical results in Fig. 3(e) are in correspondence with the phonon number distribution in Fig. 3(c), and explain its bimodal character. Similar oscillator instabilities have been used as the basis for a sensitive readout scheme in superconducting qubits [34], and may potentially be useful for mass or magnetic field sensing applications where small changes of frequency need to be detected.

To predict the oscillator response to be detected via a charge sensor (see below), we solve for the stationary state of Eq. (4) directly for a range of driving frequencies, qubit-oscillator detunings (set by the magnetic field), and temperatures T. In Figs. 3(g) and 3(h), we show the $T = 0$ and $T = 50$ mK root mean squared oscillator amplitude $X \propto \sqrt{\bar{n} + 1/2}$ as function of magnetic field B and drive frequency, for the case of a spin (S) qubit. The value $\delta B = 0$ corresponds to resonant coupling $\omega_q = \omega_p$. These results also apply for the Kx qubit, if the magnetic field axis is adjusted appropriately. In the zero-temperature case, only half of the eigenstates $\hbar\omega_\pm \approx \hbar\omega_p \mp \hbar g^2/(\omega_p - \omega_q)$ of Eq. (3) can be efficiently excited by the drive at fixed δB, giving rise to the upper (lower) feature in Fig. 3(g) for $\delta B < 0 (\delta B > 0)$. However, for $T \gtrsim \hbar\omega_q$, both branches of the Jaynes-Cummings ladder can be efficiently excited [Fig. 3(h)]. This is a distinct and experimentally accessible signature of the strong coupling at finite temperature. Note that the vacuum Rabi splitting is also observed [see arrows in Fig. 3(d)], but features arising from nonlinearity in the strongly driven system dominate by more than 2 orders of magnitude.

Displacement detection of nanomechanical systems is possible using charge sensing [5,35], where the conductance of a mesoscopic conductor, such as a QD or quantum point contact, is modulated via capacitve coupling to the charged mechanical resonator. Furthermore, the qubit state itself can be read out using spin-detection schemes developed for semiconductor QDs [36], or by a dispersive readout scheme like that commonly used in superconducting qubits coupled to microwave resonators [37]. The dispersive regime can be rapidly accessed by, e.g., tuning the resonator frequency using dc gate pulses which control the tension in the CNT [4].

In summary, we predict that strong qubit-resonator coupling can be realized in suspended CNT QDs with current state-of-the-art devices. The coupling described here may find use in sensing applications, and in spin-based quantum information processing, where the CNT oscillator enables electrical control of the electron spin, and, with capacitive couplers, may provide long-range interactions between distant electronic qubits [16,38]. Combined with control of the qubit via electron-spin-resonance [39], the mecha-

nism studied here could be utilized for ground-state cooling and for generating arbitrary motional quantum states of the oscillator [15].

We gratefully acknowledge helpful discussions with H. Carmichael, V. Manucharyan, and P. Rabl. This work was supported by the OTKA grant PD 100373, the Marie Curie grant CIG-293834 and the QSpiCE program of ESF (A. P.), DFG under the programs FOR 912 and SFB 767 (P. S. and G. B.), NSF grants DMR-090647 and PHY-0646094 (M. R.), and The Danish Council for Independent Research–Natural Sciences (K. F.).

While completing this manuscript, we became aware of a related work [40] that describes the theory of the spin-phonon coupling in a CNT resonator QD, and its consequences in the spin blockade transport setup.

[1] A. D. O'Connell, M. Hofheinz, M. Ansmann, R. C. Bialczak, M. Lenander, Erik Lucero, M. Neeley, D. Sank, H. Wang, M. Weides, J. Wenner, J. M. Martinis, and A. N. Cleland, Nature (London) **464**, 697 (2010).
[2] H. B. Peng, C. W. Chang, S. Aloni, T. D. Yuzvinsky, and A. Zettl, Phys. Rev. Lett. **97**, 087203 (2006).
[3] C. Chen, S. Rosenblatt, K. I. Bolotin, W. Kalb, P. Kim, I. Kymissis, H. L. Stormer, T. F. Heinz, and James Hone, Nature Nanotech. **4**, 861 (2009).
[4] G. A. Steele, A. K. Hüttel, B. Witkamp, M. Poot, H. B. Meerwaldt, L. P. Kouwenhoven, and H. S. J. van der Zant, Science **325**, 1103 (2009).
[5] H.-Y. Chiu, P. Hung, H. W. Ch. Postma, and M. Bockrath, Nano Lett. **8**, 4342 (2008).
[6] B. Lassagne, D. Garcia-Sanchez, A. Aguasca, and A. Bachtold, Nano Lett. **8**, 3735 (2008).
[7] B. Lassagne, D. Ugnati, and M. Respaud, Phys. Rev. Lett. **107**, 130801 (2011).
[8] D. Loss and D. P. DiVincenzo, Phys. Rev. A **57**, 120 (1998).
[9] J. R. Petta, A. C. Johnson, J. M. Taylor, E. A. Laird, A. Yacoby, M. D. Lukin, C. M. Marcus, M. P. Hanson, and A. C. Gossard, Science **309**, 2180 (2005).
[10] B. Trauzettel, D. V. Bulaev, D. Loss, and G. Burkard, Nature Phys. **3**, 192 (2007).
[11] D. V. Bulaev, B. Trauzettel, and D. Loss, Phys. Rev. B **77**, 235301 (2008).
[12] P. R. Struck and G. Burkard, Phys. Rev. B **82**, 125401 (2010).
[13] A. Cottet and T. Kontos, Phys. Rev. Lett. **105**, 160502 (2010).
[14] D. Rugar, R. Budakian, H. J. Mamin, and B. W. Chui, Nature (London) **430**, 329 (2004).
[15] P. Rabl, P. Cappellaro, M. V. Gurudev Dutt, L. Jiang, J. R. Maze, and M. D. Lukin, Phys. Rev. B **79**, 041302(R) (2009).
[16] P. Rabl, S. J. Kolkowitz, F. H. L. Koppens, J. G. E. Harris, P. Zoller, and M. D. Lukin, Nature Phys. **6**, 602 (2010).
[17] T. Ando, J. Phys. Soc. Jpn. **69**, 1757 (2000).
[18] J. S. Jeong and H. W. Lee, Phys. Rev. B **80**, 075409 (2009).
[19] W. Izumida, K. Sato, and R. Saito, J. Phys. Soc. Jpn. **78**, 074707 (2009).
[20] J. Klinovaja, M. J. Schmidt, B. Braunecker, and D. Loss, Phys. Rev. Lett. **106**, 156809 (2011).
[21] F. Kuemmeth, S. Ilani, D. C. Ralph, and P. L. McEuen, Nature (London) **452**, 448 (2008).
[22] T. S. Jespersen, K. Grove-Rasmussen, J. Paaske, K. Muraki, T. Fujisawa, J. Nygard, and K. Flensberg, Nature Phys. **7**, 348 (2011).
[23] A. Pályi and G. Burkard, Phys. Rev. Lett. **106**, 086801 (2011).
[24] See Supplemental Material at http://link.aps.org/supplemental/10.1103/PhysRevLett.108.206811 for more details.
[25] G. D. Mahan, Phys. Rev. B **65**, 235402 (2002).
[26] E. Mariani and F. von Oppen, Phys. Rev. B **80**, 155411 (2009).
[27] M. S. Rudner and E. I. Rashba, Phys. Rev. B **81**, 125426 (2010).
[28] K. Flensberg and C. M. Marcus, Phys. Rev. B **81**, 195418 (2010).
[29] A. K. Huttel, G. A. Steele, B. Witkamp, M. Poot, L. P. Kouwenhoven, and H. S. J. van der Zant, Nano Lett. **9**, 2547 (2009).
[30] H. O. H. Churchill, F. Kuemmeth, J. W. Harlow, A. J. Bestwick, E. I. Rashba, K. Flensberg, C. H. Stwertka, T. Taychatanapat, S. K. Watson, and C. M. Marcus, Phys. Rev. Lett. **102**, 166802 (2009).
[31] E. T. Jaynes and F. W. Cummings, Proc. IEEE **51**, 89 (1963).
[32] P. Alsing and H. J. Carmichael, Quantum Opt. **3**, 13 (1991).
[33] L. S. Bishop, E. Ginossar, and S. M. Girvin, Phys. Rev. Lett. **105**, 100505 (2010).
[34] M. D. Reed, L. DiCarlo, B. R. Johnson, L. Sun, D. I. Schuster, L. Frunzio, and R. J. Schoelkopf, Phys. Rev. Lett. **105**, 173601 (2010).
[35] R. G. Knobel and A. N. Cleland, Nature (London) **424**, 291 (2003).
[36] See, e.g., J. M. Elzerman, R. Hanson, L. H. Willems van Beveren, B. Witkamp, L. M. K. Vandersypen, and L. P. Kouwenhoven, Nature (London) **430**, 431 (2004).
[37] A. Wallraff, D. I. Schuster, A. Blais, L. Frunzio, J. Majer, M. H. Devoret, S. M. Girvin, and R. J. Schoelkopf, Phys. Rev. Lett. **95**, 060501 (2005).
[38] A. Imamoglu, D. D. Awschalom, G. Burkard, D. P. DiVincenzo, D. Loss, M. Sherwin, and A. Small, Phys. Rev. Lett. **83**, 4204 (1999).
[39] F. H. L. Koppens, C. Buizert, K. J. Tielrooij, I. T. Vink, K. C. Nowack, T. Meunier, L. P. Kouwenhoven, and L. M. K. Vandersypen, Nature (London) **442**, 766 (2006).
[40] C. Ohm, C. Stampfer, J. Splettstoesser, and M. Wegewijs, Appl. Phys. Lett. **100**, 143103 (2012).